Journal of Cultural Heritage 80 (2026) 263–271

Contents lists available at ScienceDirect

Journal of Cultural Heritage

journal homepage: www.elsevier.com/locate/culher

VSI: TECHNART 2025

Unveiling the maniz. cod. 99: A microscopic and spectroscopic investigation of its writing inks

Margarida Nunes[a,b,*], Victoria Corregidor[c], Luís C. Alves[c], Bruno J.C. Vieira[c], João Carlos Waerenborgh[c], Scott G. Mitchell[d], Ana Claro[e], Teresa Ferreira[a,f,*]

[a] University of Évora, HERCULES Laboratory/IN2PAST, Portugal
[b] University of the Basque Country, Department of Analytical Chemistry, Faculty of Pharmacy, Vitoria-Gasteiz, Spain
[c] C²TN, Centro de Ciências e Tecnologias Nucleares, DECN, Instituto Superior Técnico, Universidade de Lisboa, E.N. 10, km 139.7, 2695-066 Bobadela LRS, Portugal
[d] INMA-CSIC/UNIZAR - Instituto de Nanociencia y Materiales de Aragón, Consejo Superior de Investigaciones Científicas-Universidad de Zaragoza, Spain
[e] CHAM-Centre for the Humanities, College of Social and Human Sciences, NOVA Universidade de Lisboa, Portugal
[f] University of Évora, Sciences and Technology School, Chemistry and Biochemistry Department, Portugal

ARTICLE INFO

Article history:
Received 12 December 2025
Accepted 26 May 2026

Keywords:
Iron gall ink
Vitriol
Zn-rich ink
IGI-induced paper degradation
Mössbauer spectroscopy

ABSTRACT

The *Orthographia Pratica de Varias Letras* is a unique 17th-century Portuguese codex, notable for its exceptional significance in the history of Latin calligraphy during the Modern period. Unfortunately, it faces complex conservation challenges due to the presence of iron gall ink (IGI). This work aimed to thoroughly characterise the inks and their impact on the manuscript using an integrated analytical approach. Extensive micro-XRF analysis revealed two distinct groups of IGIs based on their transition metal content. Zn-rich IGIs were found in half of the manuscript, suggesting the use of Zn-bearing green vitriol. In contrast, a more refined form of green vitriol was identified in the IGIs on the other half, suggesting that different types of vitriol were used. Variations in the binder-to-vitriol ratios were proposed, indicating distinct IGI formulations throughout the codex. The poor condition observed in some folios was primarily associated with greater ink coverage per surface area and lower binder content. FIB-SEM and PIXE analysis provided insights into the behaviour of Fe within the cellulose structure, including penetration and lateral migration. The IGI chromophore was further investigated by Mössbauer and XPS, which confirmed an Fe(III)-polyphenol mono-complex with a catecholate binding mode and Fe(III) in an octahedral arrangement.

1. Introduction and research aim

Iron gall ink (IGI) was the favoured writing medium in European Medieval *scriptoria* due to its permanence and variable black shades [1]. Produced from gallnuts (rich in polyphenolic compounds) and green vitriol (iron-rich salts), IGI formulations often included binders and additives to adjust characteristics, such as viscosity and shade or hue [2]. Studies on IGI have focused on metal composition, particularly minor element-to-Fe ratios, with Zn-containing inks providing evidence for historical vitriol trade and IGI formulation practices [3–5]. Complementary studies using historical reproductions have advanced knowledge on the chemistry behind the colourant, i.e., metal–polyphenol complexation, and the mechanisms driving IGI-induced decay [6–8]. Research has increasingly focused on the latter aspect, as IGIs are now recognised to potentiate the two main mechanisms of cellulose degradation: acid-catalysed hydrolysis and metal-catalysed oxidation, posing significant conservation challenges for the written heritage [9–11]. In this context, the critical role of Fe, particularly its migration within the substrate, has received particular attention [12–14].

Ortographia Pratica de Varias Letras (maniz. cod. 99), a 17th-century manuscript authored by the Jesuit priest António Pessoa and dedicated to D. Teodósio (1634–1653), heir to the House of Bragança [15], is a relevant manuscript to the history of Latin calligraphy in the early Modern period but has remained overlooked. Its current condition mirrors the contrasting scenarios often encountered on IGI documents: while most folios are well-preserved, a central section exhibits severe damage [15]. This work investigates ink composition and its variability across folios, migration patterns within the writing support, and potential correlations with the observed conservation state, using a multi-analytical

* Correspnding authors.
E-mail addresses: mrmpn@uevora.pt (M. Nunes), tasf@uevora.pt (T. Ferreira).

https://doi.org/10.1016/j.culher.2026.05.019

strategy. More broadly, it also intends to highlight the significance and exceptional quality of the maniz. cod. 99 through a material-based analysis, while raising awareness of its current condition, and advocating for targeted preservation measures.

2. Material and methods

2.1. Sampling object

The maniz. cod. 99 (Fig. SM.1) was thoroughly examined for its physical and anatomical features, along with targeted sampling. A complete description is provided in the Supplementary Material (SM), Section 2.1.

The manuscripts' quill penwork and writing were classified into three categories according to function, and inks were studied accordingly: i) text block – the main written text; ii) calligraphic writing - fine writing in the various alphabet scripts, concentrated in ff. 98, 99, 119–156 (excluding ff. 128–129); iii) decorations – ornamental motifs in bar borders and within the writing space.

Sampling was limited to fragile areas within the damaged set of folios (ff. 119–156) (Table 1). Loosened ink fragments were compiled from the gutter (ff. 148–151 and 154–157) for Mössbauer measurements. In addition, three sacrificial samples were collected from the bottom edge of well-preserved folios (ff. 5, 30 and 159) to characterise the paper support.

2.2. Analytical characterisation

A detailed description of the analytical instrumentation and methodology is given in the SM (Supplementary Material, Section 2.2).

3. Results and discussion

3.1. Paper support

The paper support is a handmade historical paper, produced from vegetable bast fibres, of fine thickness, and presenting a laid ('antique') pattern. It is characterised by a fine texture, slight surface roughness, and an off-white to pale yellowish tone. A comprehensive characterisation of the support and discussion is available in the SM (Section 3.1, Fig. SM.2–3 and Table SM.1).

3.2. The inks – hue, composition, and degradation

Visual inspection showed that inks ranged from a light rusty-brown in the text block and some decorations (Fig. 1a, b) to darker hues in fully inked calligraphic letters, often outlined and filled with parallel dashes. Colourimetric measurements confirmed these observations with higher L* values for the block text and lower a* and b* values for the calligraphy. A distinctive golden-brown hue was observed in the text block in f. 267 (Fig. 1b), characterised by increased a* and b* contributions, a likely personal addition containing an unframed, self-praising sonnet dedicated to the Prince of Portugal.

Ink hue and shade variations were systematically analysed across 46 folios (Table SM.2), considering three categories of ink use: text block, decorations and calligraphic writing. The darkest shades (lower L* values) were consistently observed in calligraphic writing, reflecting the higher ink deposition per surface area. In contrast, the text block and decorations featured lighter shades, with the text block additionally characterised by a slight yellowish hue. Further discussion is available in the SM (Section 3.2).

In situ micro-XRF analyses were performed on quill penworks across 38 folios (Table SM.3) to assess ink metal content, with folio conservation state evaluated using Reissland and Hofenk de Graaf's classification system [16]. Representative XRF spectra from uninked and inked areas in ff. 13 and 170 are shown in Fig. SM.4. The IGI nature of the writing was suggested by the systematic presence of Fe in the inked areas, along with the IR insights presented in Fig. SM.5 and Table SM.4. Although the spectra discussed in Fig. SM.5 show contributions from the cellulose matrix, several features exhibit characteristic differences in shape and intensity, consistent with IGI, as supported by the literature [6,17].

Alongside Fe, elements commonly associated with IGIs, such as K, S, Ca, Mn, Cu and Zn, were detected. Among these, S, Mn, Fe, Cu, and Zn can be attributed to the vitriol component [18], whereas K and Ca are consistent with a polysaccharide binder, most likely Arabic gum [19], although both elements may also have contributions from the gallnuts [20]. The Ca signal, however, is not specific to the ink. The comparable peak intensities in inked and uninked areas in f. 13 (Fig. SM.4) suggest a substantial background contribution from the paper substrate, most likely introduced during manufacture. This needs to be kept in mind when interpreting Ca-based indicators. The distribution of Fe:Rh normalised count ratios across the 38 folios is presented in Fig. 2a. The most severe deterioration occurred in ff. 119–156, particularly ff. 118–119 and 143–156, which also exhibited the highest Fe levels (Rh-normalised), consistent with the greater ink load per surface area observed in calligraphic writing.

To explore whether binder content varies with conservation state, K:Fe and Ca:Fe count ratios (Rh-normalised) were calculated (Fig. SM.6). The procedure minimises the influence of ink layer thickness and surface topography and allows a more direct comparison between areas of different ink loads. The lowest K:Fe and Ca:Fe count ratios (Rh-normalised) coincided with the highest Fe intensities (Rh-normalised) associated with folios in poor to bad condition. The interpretation is not straightforward, as Ca and K may also derive from other sources. Nevertheless, K contribution from gallnuts is expected to be variable but not systematically correlated with Fe, and therefore unlikely to explain consistent trends in K:Fe count ratio across folios. As for Ca, its main contribution comes from the paper support, suggesting it will be relatively homogeneous across the manuscript. Consequently, while Ca and K absolute signals may include a background component unrelated to the binder, their distribution from other components does not compromise the observed trends for K:Fe and Ca:Fe ratios, which remain meaningful for comparative purposes across the folios. In this context, the observed decrease in Ca:Fe, and especially in the K:Fe count ratios, is possibly best understood as reflecting a leaner binder formulation in the most degraded areas. Accordingly, these correlations should be interpreted as indicators of relative variations in binder content across the folios.

Raw vitriol is key for distinguishing the IGIs' transition-metal composition [21,22]. It forms naturally in mining environments through the oxidation of Fe-, Cu-, and Zn-bearing sulfides (e.g., pyrite, chalcopyrite, sphalerite), yielding secondary sulfate minerals enriched in divalent cations, such as melanterite, chalcanthite, and goslarite [23,24]. Green vitriol, historically associated with IGI production, is now identified as melanterite ($FeSO_4{\cdot}7H_2O$), the pure Fe(II) sulfate end-member. However, historical vitriols were rarely pure and typically contained variable amounts of Cu, Zn and Mn, reflecting both the mineralogical origin of the ore and the extraction or processing methods employed [18,25,26]. A detailed discussion is provided in the SM (Section 3.2. *Discussion on vitriols*).

To assess the presence of Mn and Cu as impurities or elements of interest in the inks, Rh-normalised Mn:Fe and Cu:Fe count ratios were calculated (Fig. 2b and c). From the graphs' evaluation, two distinct groups were considered: i) ff. 5–153, exhibiting lower Mn:Fe and Cu:Fe count ratios (group 1); ii) ff. 156 onwards, showing generally higher ratios (group 2). Overall, Mn:Fe count ratios consistently remained below ~10%, and Cu:Fe did not exceed ~9%.

Table 1
Sample identification code (id), corresponding folio, 3D digital microscopic image, and brief description of the samples.

sample id	folio no.	3D digital image	description
1	5		uninked area of the paper support, bottom edge
2	119		calligraphic writing, Latin alphabet ('E'), middle of text block
3			calligraphic writing, Latin alphabet ('G'), middle of text block
4	120		calligraphic writing, Latin alphabet ('U'), middle of text block
5	137		calligraphic writing, Mouresc alphabet (letter *cof*), folio bottom
6			calligraphic writing, Mouresc alphabet (letter *guau*), folio bottom
7	148	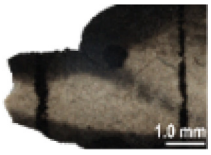	calligraphic writing, Latin alphabet (unidentified letter), middle of text block
8	156		decoration, middle of text block
9	148–151		loosened inked fragments accumulated in the gutter
10	154–157		

Similar Mn:Fe count ratios (6–10%) reported in other IGI studies [26,27] support the interpretation of Mn as a vitriol impurity. Based on this threshold, element-to-Fe ratios below 10% were considered indicative of impurities. Accordingly, the Cu:Fe count ratios also rule out the deliberate use of Cu-containing blue vitriols.

Similarly, the Zn:Fe count ratios (Fig. 2d) revealed the same bimodal distribution observed for the other elemental ratios. Two distinct groups can be defined: group 1 displayed Zn:Fe count ratios ranging from 7% to 16%, with ca. 65% of values below the 10% threshold, whereas group 2 had a minimum count ratio of 11%, and predominantly higher values, most above 25%. Overall, Zn:Fe ratios in group 2 roughly double those in group 1. As for the uninked areas, Zn ws observed at low levels (Fig. SM.4), with Zn:Rh normalised count ratios below ~2 and no significant variation within or between the two groups. This uniform background is consistent with expectations for a 17th-century paper support and does not justify correction of the Zn signal. Consequently, the differences observed in the inks must therefore reflect their formulation rather than the support. Interestingly, the Zn-rich inks in group 2 are not enriched in Zn alone but also show higher Mn:Fe and Cu:Fe count ratios, indicating a systematic co-enrichment of these elements. Such a compositional pattern strongly suggests the use of distinct vitriol batches or types, likely reflecting variability in raw materials types.

No systematic correlation was observed between metal composition and ink hue, since the two Zn:Fe groups do not correspond to hue variations, which instead follow the ink load primarily. The golden-brown ink on folio 267 is an example which further illustrates this point: despite its distinctive appearance, its elemental composition falls within group 2, indicating that the inorganic fraction alone cannot account for the observed hue differences. Since hydrolysable tannins exhibit a lower affinity for Zn(II) than for Fe(II) and Cu(II) ions [28], Zn is unlikely to influence substantially the PPh-metal complexes responsible for colour for-

Fig. 1. Photographic details, 3D digital microscopic images illustrating morphological aspects of representative inked areas and corresponding average L*a*b* values and std (σ) values. Text block with a) rusty-brown hue (f. 24); and b) golden brown hue (f. 267); c) calligraphic writing with a dark black shade (f. 127).

mation. Differences in the phenolic profile of the galls, extraction procedures, and/or ageing processes must therefore be responsible for the different hue observed on folio 267. Likewise, no relationship between Zn content and folio conservation state was observed. Severely degraded folios (ff. 119–156), including f. 156, as well as the better-preserved folios (e.g., ff. 161, 164, 170), are all associated with Zn-rich inks (Table SM.3), indicating that high Zn:Fe ratios do not measurably mitigate IGI-induced degradation. Owing to its filled 3d subshell, Zn(II) ion is not redox-active under typical IGI conditions, preventing it from participating in metal-catalised oxidative pathways associated with IGI-induced degradation. Overall, the results provide no evidence for a functional role of the Zn(II) ion in relation to either ink colour or preservation state.

The only known examples of Zn-containing IGIs in Portuguese documentation are noted in Tibúrcio et al. [4] and Manso et al. [29], consistent with our recent study on the documentation of the General Council of the Portuguese Inquisition [5]. Zn-rich IGIs have been reported in Bohemian [30] and late Medieval Flemish manuscripts [3], leading to their association with Northern Europe. However, goslarite (Zn sulfate, white vitriol) is scarcely found in historical IGI recipes [31], since Zn-polyphenol (Zn-PPh) compounds are unlikely to affect ink hue, making their deliberate use improbable. According to Vuillard et al. [32], distinguishing vitriol variants by their hue is challenging, but feasible. Laboratory experiments replicating historical recipes with varying Zn:Fe ratios demonstrated that Zn content affects vitriol hue, from green (low Zn) to light turquoise (higher Zn). This remark is supported by geological knowledge, noting that vitriol makers were likely familiar with compositional variations producing hue variation. Thus, the presence of Zn-rich vitriols in IGI may reflect the natural variability and commercial circulation of mixed sulfate minerals rather than any deliberate formulation strategy.

Table 2
Parameters estimated from the Mössbauer spectra taken at 295 K of sample 9 (ff. 148–151) and sample 10 (ff. 154–157).

sample id	Fe species	IS (mm s^{-1})	QS (mm s^{-1})	I
9	Fe(III)	0.38	0.72	85%
	Fe(II) oxalate	1.20	1.76	15%
10	Fe(III)	0.39	0.75	82%
	Fe(II) oxalate	1.21	1.75	18%

Isomer shift (IS) relative to metallic α-Fe at 295 K; quadrupole splitting (QS); relative areas (I). Estimated errors are $\leq$ 0.02 mm s^{-1} for IS, QS, and $\leq$ 2% for I.

Mössbauer measurements on samples 9 and 10 (Table 2) were performed to assess the Fe coordination environment and its oxidation state. The obtained spectra are similar within experimental error (Fig. SM.7, Table 2). They may be fitted with two quadrupole doublets: the doublet with a lower isomer shift (IS) relative to metallic Fe at room temperature (RT) and lower quadrupole splitting (QS) is typical of Fe(III); the other doublet has IS and QS characteristics of Fe(II).

Fe(III) was identified as the principal component, while a smaller Fe(II) percentage of Fe(II) was also detected and assigned to Fe(II) oxalate. In their investigation of three 18th-century books (Chancery MS, Latin MS Letters, and a cookbook), Lerf et al. [33] likewise found that virtually all iron was present as Fe(III).

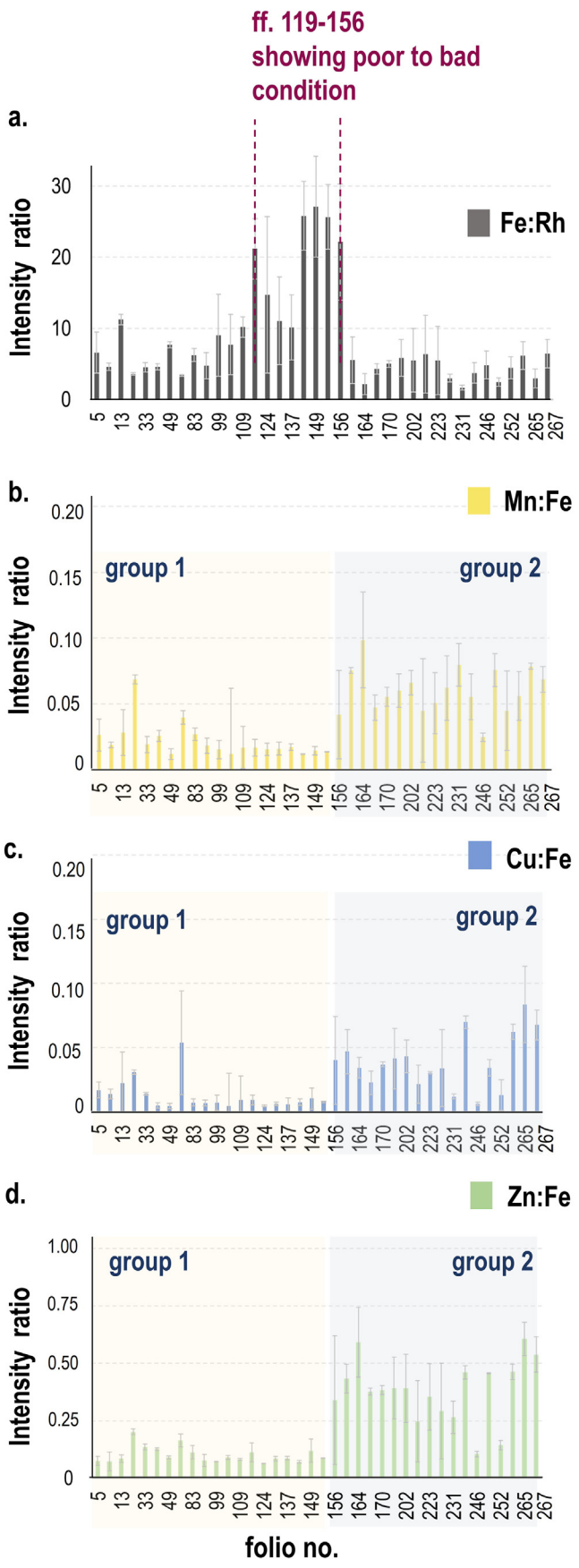

Fig. 2. a) Fe:Rh normalised count ratios; b) Mn:Fe, c) Cu:Fe, and d) Zn:Fe count ratios (Rh-normalised) distribution along 38 folios corresponding to the inked areas indicated in Table SM.3.

Nevertheless, the authors [33] were unable to assign the ferric quadrupole doublet observed in all manuscripts to any compound, namely iron gallate, suggesting that different PPh ligands have complexed the Fe(III) ion. Besides, Fe(II) oxalate was also found in the Chancery MS. As in Lerf et al. (2021) [33] investigation, the parameters of the ferric doublets in our samples do not correspond to those of either synthetic crystalline or amorphous Fe-gallate, the dominant IGI chromophore model in the literature for decades [34–37]. Both works are in line with what was recently reported [7,38], attesting that the IGI complex may also be composed of galloyl esters of glucose (e.g., pentagalloylglucose and hexagalloylglucose) and cannot be solely represented as a simple Fe-gallate complex. Notably, the Fe(III) parameters obtained in this study are, within experimental error, similar to those reported for a Fe(III)-PPh mono-complex formed from $Fe_2(SO_4)_3 \bullet nH_2O$ and oak tannin [39]. The study showed that complex formation required at least two -OH groups in *ortho* position on the aromatic ring of the PPh ligand (catecholate moiety), whereas the total number of phenolic groups and the specific ligand backbone of the PPh did not affect the Mössbauer parameters. This suggests that the IGI complex in our samples corresponds to a Fe(III)-PPh mono-complex coordinated via catecholate functionalities, in agreement with our previous findings [17].

The formation of Fe(III)-PPh mono-complexes was exclusively observed at low pH values (pH $\leq$ 3), similar to the typical environment of IGIs [40,41]. Although most phenolic groups have pKa values in the range 7–10, deprotonation can occur in acidic solutions in the presence of strong Lewis acids like Fe(III) [42,43]. In contrast, the weaker Lewis acid Fe(II) forms less stable Fe(II)-PPhs complexes that readily undergo autooxidation promoted by the PPh ligands. During this process, the PPhs can be oxidised to semiquinone species, accompanied by proton release and a decrease in the Fe reduction potential [44]. Ligand field considerations further support this behaviour: neutral unsaturated ligands tend to stabilise Fe(II) (d^6) over Fe(III) (d^5) due to greater crystal field stabilisation energy. However, the close proximity of the Fe(III)/Fe(II) reduction potential (0.749 V) to that of many PPhs (*o*-quinone/PPh) redox couples [41] facilitates electron transfer between metal and ligand, promoting redox cycling and ultimately, complete oxidation of PPhs to quinones [42,44]. Our Mössbauer study could not associate Fe(II) species with quinone ligands; instead, they were paired with oxalate. Mössbauer parameters for Fe(II) oxalate (IS $\approx$ 1.20 mm s^{-1}; QS $\approx$ 1.76 mm s^{-1}) are in good agreement with the values obtained in Lerf et al.'s study [33].

As previously observed [17], the Fe(II) phase develops over time at the expense of Fe(III) species. Oxalic acid may form through the oxidative degradation of carbohydrates such as cellulose and Arabic gum [33], or via microbial activity, through oxalate secretion mediated by oxalate oxidase [45,46]. SEM observations confirmed microbial colonisation of the samples (Fig. SM.8), supporting this pathway. Previous studies [47] have identified distinct Fe oxalates on the surface of IGI layers, interpreted as secondary degradation products.

3.3. IGI surface and penetration into the support

XPS analysis was performed to characterise the surface chemical composition of IGI using loosened fragments from samples 3 (f. 119), 4 (f. 120), 7 (f.148), and 10 (f. 154), all of which feature calligraphic writing. Survey spectra are shown in Fig. 3. The analysis was restricted to the Fe 2p and C 1 s regions. Sample 3 was selected as representative, and its spectra are presented in Fig. 3b,c. Curve fitting of the Fe $2p_{3/2}$ and C 1 s regions were performed to gain further insights into the surface chemical composition, namely, the Fe coordination environments and carbon-containing functionalities at the surface.

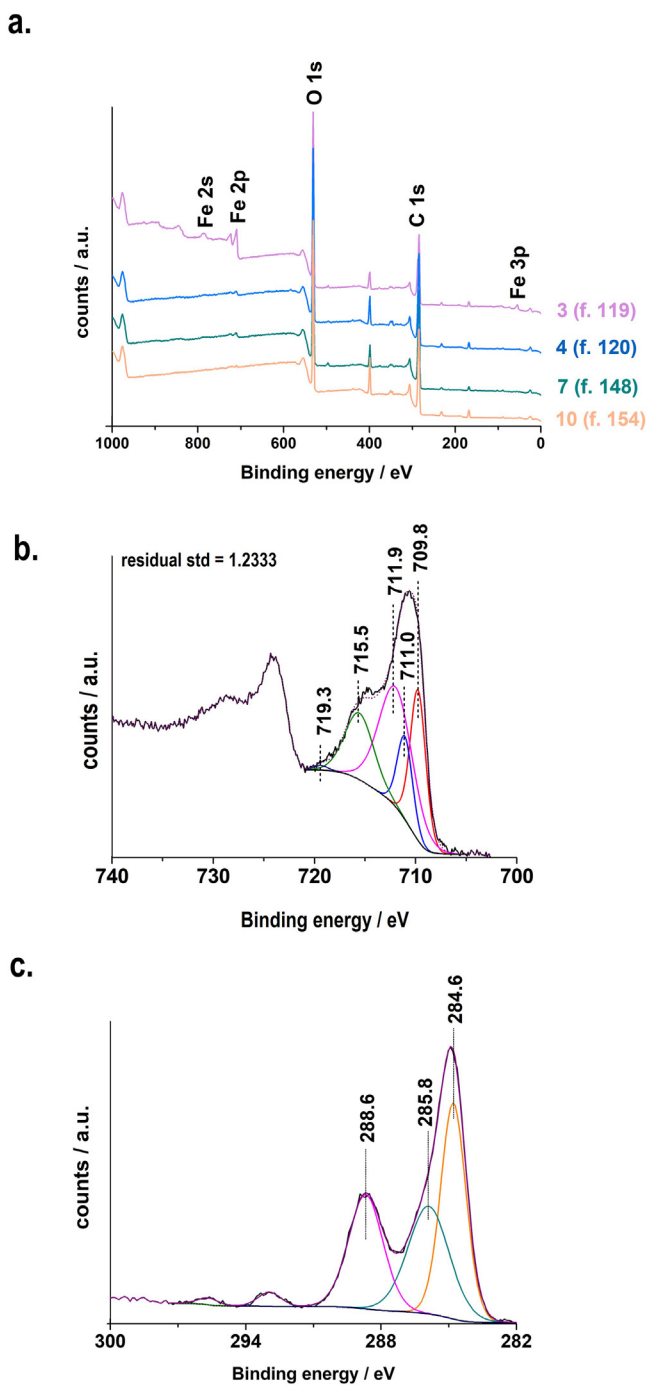

Fig. 3. a) XPS survey spectra of samples 3, 4, 7, 10; curve fitting of sample 3 spectra with peak position marked: b) Fe 2p region; c) C 1 s and K 2p regions. The experimental spectra, background line, and the envelope of the fitting components are shown.

The Fe $2p_{3/2}$ envelope was fitted following the fitting methodology proposed by Biesinger et al. [48] for siderite (a mineral composed of iron carbonate), including multiplet splitting and satellite contributions characteristic of Fe compounds. The envelope comprises three principal components centred at 709.8, 711.0, and 711.9 eV, together with two satellites at 715.5 and 719.3 eV (Table SM.5). Overall, the peak envelope between 709 and 720 eV is consistent with the multiplet splitting previously reported for Fe in oxides, hydroxides, sulfates, oxalates and carbonates [48–51]. The lower binding energy components at 709.8 and 711.0 eV are consistent with Fe(II) containing species. The peaks at 709.6 and 715.5 eV are in good agreement with the reported binding energies for standard siderite ($FeCO_3$), centred at ~710.2 with a satellite near 714.9 eV (C $1s_{carbonates}$ = 289.4 eV and C $1s_{adsorbed\ hydrocarbons}$ = 284.6 eV, Mg Kα radiation source) [52]. Besides, the value of 710.4 eV was also found for the main peak in Fe(II) oxalates (C 1 s $_{adventitious}$ = 285 eV, Mg Kα radiation source) [51].

Descostes et al. [53] characterised Fe(II) in hydrated iron (II) sulfate ($FeSO_4{\cdot}7H_2O$) with a melanterite-type structure, in which Fe(II) is octahedrally coordinated by six H_2O molecules [54]. The reported Fe $2p_{3/2}$ main and satellite peaks at 711.0 eV and 715.3 eV (C 1s = 284.60 eV), respectively, are in good agreement with the features observed in the present study. Hence, the peak at 711.0 eV is consistent with hydrated Fe(II) sulfate, while the satellite at 715.5 eV can also arise from this compound, as it does in the case of siderite. Iron (II) sulfate is commonly found in IGI due to the reduction of Fe(III) in the Fe(III)-PPh complex, which can then react with available sulfate ions [17]. In these structures, Fe(II) is octahedrally coordinated by oxygen, forming FeO_6 environments. Significant overlap exists among these Fe(II) species, potentially including sulfate, carbonate and oxalate. These results are in good agreement with our Mössbauer results, in which the presence of Fe(II) oxalates was estimated.

Higher binding energy components are attributed to Fe(III). Allen and Hallam [55] analysed the Co-containing ferrite spinel series ($Fe_xCo_{1-x}Fe_2O_4$, $0 \leq x \leq 1$) and observed that the main Fe $2p_{3/2}$ peak position shifted toward lower BE values when Fe(II) substituted Co(II) in the series, with the highest BE value obtained for $CoFe_2O_4$, where Fe is only present as Fe(III). The authors reported a similar trend for the Mn-Fe and Ni-Fe spinel series: the Fe $2p_3/_2$ binding energies obtained for x = 0 in the three series were 711.2, 711.6 and 711.3 eV, respectively, (with C 1s = 285.0 eV). Based on these observations, the higher-BE component in the current study at 711.9 eV, together with a satellite at 719.3 eV, agrees well with Fe(III) in an octahedral coordination environment, as reported by Atrei et al. [56]. Combined with the Mössbauer results, this confirms the interpretation that Fe(III) in the IGI is predominantly present as an octahedrally coordinated Fe-PPh complex. The C 1 s region is further discussed in the SM (Section 3.3 *XPS analysis*).

While XPS provided insights into the Fe speciation at the ink surface, PIXE mapping highlighted differences in the spatial distribution of Zn. PIXE elemental mapping (Fig. SM.9a) showed that Zn is heterogeneously distributed, occurring as locally concentrated domains rather than as a continuous signal across the inked area. This behaviour is consistent with the findings of Karamać [28], who reported that Zn(II) ions form less stable complexes with phenolic compounds (PPh) than Fe(II) ions do. As a result, Zn(II) ions are less effectively stabilised within the Fe-PPh network and tend to accumulate locally.

SEM/EDS analysis further revealed morphological features on the ink surface, associated with Pb- and Mg-containing crystals. A detailed characterisation and proposed origin are provided in the SM (Section 3.3, *SEM/EDS and PIXE analysis*).

IGI penetration and lateral migration can result in 'strike-through' on the verso and 'haloing' around inked areas [57]. FIB-SEM and PIXE were employed to examine these phenomena. A cross-section was prepared from an inked fragment of sample 8 (f. 156) using a dual-beam FIB, avoiding the mechanical damage typical of manual preparation and enabling SEM/EDS spatial distribution analysis of IGI-characteristic elements. A fragment, measuring ca. 32.8 μm in thickness and not written or decorated on the reverse, was selected for analysis. EDS line-scan profiles showed the presence of magnesium sulfate crystals at the ink surface and their distribution within deeper layers of the paper structure. The

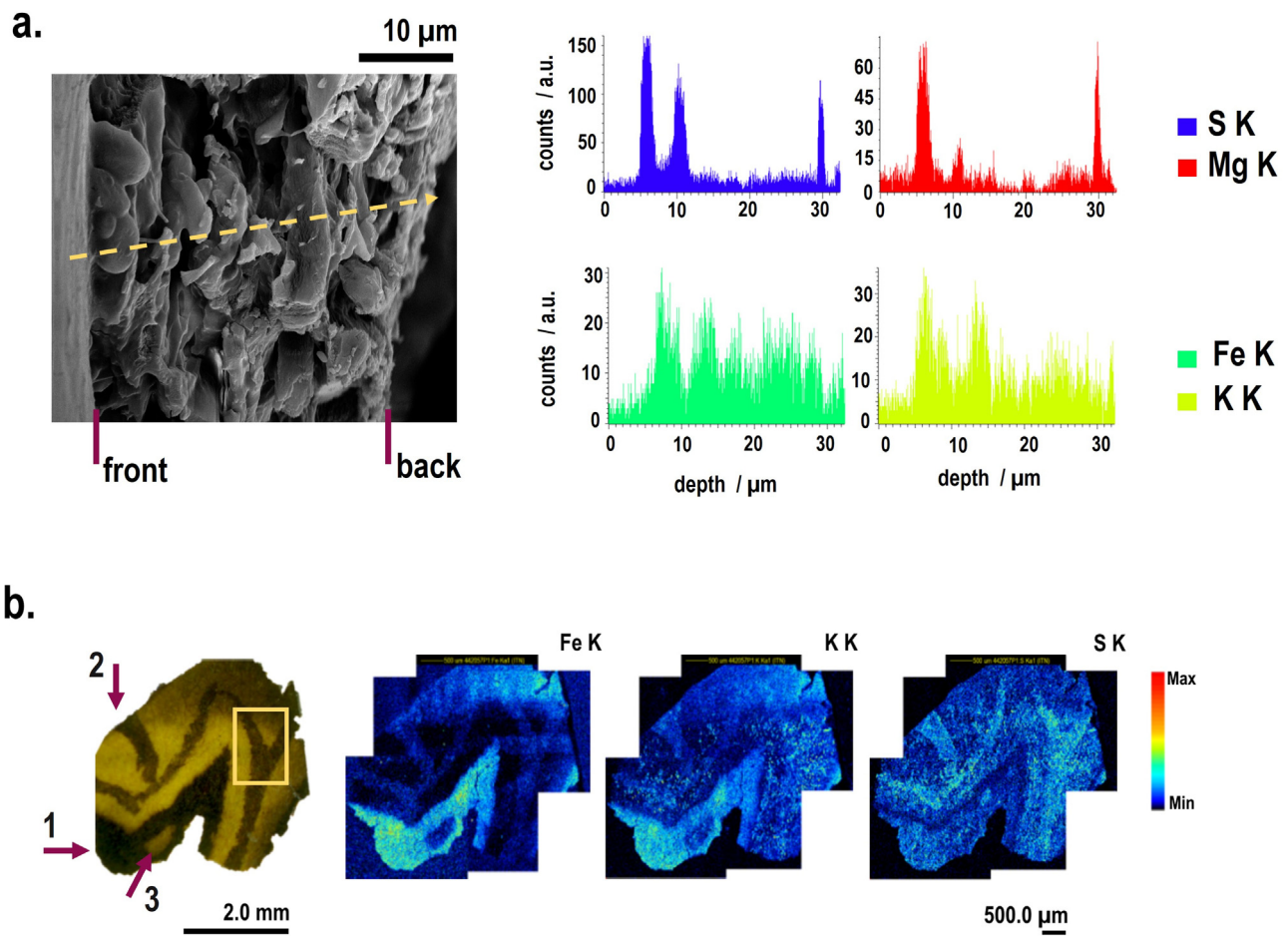

Fig. 4. a) FIB-SEM cross-section of an inked fragment from sample 8 (f. 156) and respective EDS line scan analysis showing the Fe, K, S and Mg spatial distribution; b) OM image of the sample 8 (left), with uninked and inked areas and corresponding PIXE elemental maps (2 MeV proton beam) of Fe, K and S (right). Numbers 1–3 and the yellow form are explained in the text.

S distribution closely follows that of Mg, indicating that sulfur is predominantly present as soluble sulfate species. In contrast, the weaker spatial association of S and Fe suggests that Fe is not primarily present as sulfate but as Fe-PPh or secondary phases and carbonate, corroborating the XPS observation.

Interestingly, the EDS line scans also showed a consistent decrease in Fe and K intensities from the surface towards the interior of the sample (Fig. 4a). Although both elements appeared to a lesser extent beyond *ca.* 15 µm, they were still detectable throughout the full thickness of the fragment, with the innermost region corresponding to the verso. This observation confirms the deep penetration of ink-derived ions, with complete through-thickness penetration over time. As noted above, the lower K:Fe and Ca:Fe ratios (Fig. SM.6) suggest a relatively low binder content in this folio, facilitating deeper penetration of Fe species within the cellulose matrix.

Folio 156 is decorated with partially filled inked motifs combined with fine-line quill penwork elements. The verso (f. 155) contained calligraphic writing, including a handwritten calligraphic alphabet letter positioned in the upper section. A second fragment from sample 8 (f. 156), inked on the verso, was selected as it exhibits ink-impactful migration effects (Fig. 4b). However, since a 2 MeV proton beam penetrates up to 60 µm in IGI-containing samples [58], the resulting 2D PIXE elemental maps only enable discussion of the lateral migration of elements within and around the inked areas.

At point 1 on f. 156, a heavily inked line showed the most intense Fe signal, followed by K, while S remained comparatively weaker (Fig. 4b). In contrast, at point 2 and within the yellow-marked form, corresponding to lightly inked line decoration, S presented the dominant signal, whereas Fe was minimal. As previously discussed, this S signal can be attributed to sulfate species, including iron sulfate, and more prominently to Mg sulfate. Furthermore, the dispersed distribution of S across the elemental map supports the presence of Mg sulfate crystals at the surface. Interestingly, S and K showed lateral migration towards the adjacent lightly inked areas. In contrast, Fe did not follow this pattern as illustrated in point 3. Overall, Fe lateral migration most likely occurred during the initial stage of ink penetration into the cellulose support, with minimal subsequent redistribution. In contrast, sulfate species exhibited higher mobility and accumulated in lightly inked areas.

4. Conclusions

This work employed an integrated multi-analytical approach to explore thoroughly historical IGIs in a unique 17th-century Portuguese codex, *Ortographia Pratica de Varias Letras* (maniz. cod. 99). The primary goal was to characterise the inks and assess potential correlations between their composition and the severe degradation observed in ff. 119–156.

The folios are made of high-quality rag paper composed of linen/hemp fibres and sized with a proteinaceous material (e.g. gelatine), consistent with 17th-century paper featuring gilded edges. Colourimetric analysis confirmed that areas of calligraphic

writing, which contain a higher ink load per surface area, exhibit darker, cooler hues.

All inks were identified as IGI, regardless of appearance or usage. Two main compositional groups emerged based on Zn:Fe ratios: the first (ff. 5–153) is characterised by ratios mostly ≤10%, while the second (ff. 156–267) showed higher values (11–50%), suggesting the use of compositionally distinct green vitriols, likely reflecting different raw material types. The presence of Zn-containing IGI is noteworthy, as the two IGI recipes recorded in the codex (for paper and parchment) do not mention the use of Zn-rich vitriol.

Variations in K:Fe and Ca:Fe ratios indicated inconsistent binder-to-vitriol proportions across the codex. The lowest K- and Ca-to-Fe ratios occur in the most degraded folios, suggesting that a possible reduced binder content, combined with high ink load, enhanced ink penetration and contributed to folio deterioration.

Furthermore, PIXE 2D mapping and depth profiling (FIB-SEM/EDS) revealed differentiated migration behaviour: Fe preferentially penetrates deeply through the cellulosic support, reaching the verso, while K and S showed lateral migration around inked areas. Highly unbalanced IGIs, with excessive vitriol-to-gallnuts weight ratio, often yield iron sulfate as a byproduct. Although Mössbauer spectroscopy did not detect iron sulfate phases in the bulk of degraded samples, the XPS data revealed Fe(II)-containing surface environments compatible with hydrated iron sulfates, together with other overlapping Fe(II) species, including oxalates. This observation suggests that the IGIs used in this set of degraded folios were not strongly unbalanced overall, potentially aligning with the recipe for paper that Pessoa recorded in the manuscript. Additional insights into ink degradation were provided by XPS and Mössbauer spectroscopy, which showed the formation of Fe(II) oxalates, consistent with the degradation of the Fe(III)-PPh complexes and carbohydrate substrates. These combined spectroscopies also indicated that the IGI chromophores can be described as Fe(III)-PPhs mono-complexes with catecholate-type binding, in which the *ortho*-positioned OH groups bind the Fe(III) ion in an octahedral environment.

Overall, this study showed that the exceptional degradation exhibited by ff. 119–156 is related to ink formulation, high ink load, subsequent distribution within the paper matrix, particularly the penetration and mobility of Fe. The work also aimed to contribute to a deeper understanding of IGI-written heritage within the Portuguese context, raising awareness of the historical and cultural significance of the maniz. cod. 99.

Acknowledgements

The authors acknowledge Dra Zélia Parreira, Dr Vicente Fino, and Dr João Mora from the Public Library of Évora for providing access to the maniz. cod. 99. The authors wish to thank the Laboratorio de Microscopias Avanzadas (LMA) at the University of Zaragoza for the access to their instruments and expertise and to the professional support of the Interdisciplinary Thematic Platform from CSIC Open Heritage: Research and Society (PTI-PAIS). The authors also wish to thank Prof. Fernanda Olival and Dr João Xavier Matos (Aljustrel LNEG) for their contributions to the historical and geological context, respectively. The authors also thank G. Wanzeller Martins' work with the colourimetric analysis. Language models (ChatGPT and Grammarly) were used to assist with English grammar and phrasing refinement.

The research was supported by Foundation for Science and Technology (FCT) through the IronIC (PTDC/ART-HIS/32327/2017), and Holy Bodies (10.54499/2022.01486.PTDC) projects, and https://doi.org/10.54499/UID/PRR/04449/2025 (HERCULES Laboratory), 10.54499/LA/P/0132/2020 (IN2PAST), UID/04349/2023 and UID/Multi/04349/2020 (C^2TN), the PhD grant SFRH/BD/147528/2019 and additional grant attributed due to the COVID-19 pandemic crisis (COVID/BD/153467/2023). Margarida Nunes acknowledge the support through the JDC2024-053901-I grant funded by MICIU/AEI/10.13039/501100011033 and by the ESF+.

Supplementary materials

Supplementary material associated with this article can be found, in the online version, at doi:10.1016/j.culher.2026.05.019.

References

[1] G. Nehring, O. Bonnerot, M. Gerhardt, M. Krutzsch, I. Rabin, Looking for the missing link in the evolution of black inks, Archaeol. Anthropol. Sci. 13 (2021), doi:10.1007/s12520-021-01320-5.
[2] Cultural Heritage Agency of the Netherlands, The iron gall ink website. 2011. https://irongallink.org/.
[3] R. Klockenkämper, A. Von Bohlen, L. Moens, Analysis of pigments and inks on oil paintings and historical manuscripts using total reflection X-ray fluorescence spectrometry, 2000.
[4] C. Tibúrcio, S. Valadas, A. Cardoso, A. Candeias, C. Barreira, C. Miguel, On the use of EDXRF and UV–Vis FORS to unveil the production of two illuminated manuscripts from the fifteenth century Portuguese royal court, Microchem. J. 153 (2020) 104455, doi:10.1016/j.microc.2019.104455.
[5] M. Nunes, F. Olival, S.G. Mitchell, A. Claro, T. Ferreira, A holistic approach to understanding the iron-gall inks in the historical documents of the portuguese Inquisition (1570-1790), Micron 165 (2023) 103396, doi:10.1016/j.micron.2022.103396.
[6] R.J. Díaz Hidalgo, R. Córdoba, P. Nabais, V. Silva, M.J. Melo, F. Pina, N. Teixeira, V. Freitas, New insights into iron-gall inks through the use of historically accurate reconstructions, Herit. Sci. 6 (2018), doi:10.1186/s40494-018-0228-8.
[7] N. Teixeira, P. Nabais, V. de Freitas, J.A. Lopes, M.J. Melo, In-depth phenolic characterization of iron gall inks by deconstructing representative Iberian recipes, Sci. Rep. 11 (2021) 1–11, doi:10.1038/s41598-021-87969-3.
[8] C. Burgaud, V. Rouchon, P. Refait, A. Wattiaux, Mössbauer spectrometry applied to the study of laboratory samples made of iron gall ink, Appl. Phys. A Mater. Sci. Process. 92 (2008) 257–262, doi:10.1007/s00339-008-4503-5.
[9] Y. Liu, I. Kralj Cigić, M. Strlič, Kinetics of accelerated degradation of historic iron gall ink-containing paper, Polym. Degrad. Stab. 142 (2017) 255–262, doi:10.1016/j.polymdegradstab.2017.07.010.
[10] M.J. Melo, V. Otero, P. Nabais, N. Teixeira, F. Pina, C. Casanova, S. Fragoso, S.O. Sequeira, Iron-gall inks: a review of their degradation mechanisms and conservation treatments, Herit. Sci. 10 (2022) 1–11, doi:10.1186/s40494-022-00779-2.
[11] C. Remazeilles, V. Rouchon-Quillet, J. Bernard, Influence of gum arabic on iron gall ink corrosion part I: a laboratory samples study, Restaurator 25 (2004) 220–232, doi:10.1515/REST.2004.220.
[12] V. Rouchon, S. Bernard, Mapping iron gall ink penetration within paper fibres using scanning transmission X-ray microscopy, J. Anal. At. Spectrom. 30 (2015) 635–641, doi:10.1039/c4ja00358f.
[13] F.E. Wagner, A. Lerf, Mössbauer spectroscopic investigation of Fe(II) and Fe(III) 3,4,5-trihydroxybenzoates (gallates) - proposed model compounds for iron-gall inks, J. Inorg. Gen. Chem. 641 (2015) 2384–2391, doi:10.1002/zaac.201500532.
[14] M. Nunes, P. García-Orduña, E. Atrián-Blasco, J. Costa Vieira, A.P. Costa, M.E. Cabral Amaral, A. Claro, T. Ferreira, S.G. Mitchell, Polyoxometalate-ionic liquids for mitigating the effects of iron gall ink corrosion on cellulosic supports, ACS Omega 9 (2024) 36609–36621, doi:10.1021/acsomega.4c04925.
[15] M. Nunes, A. Claro, T. Ferreira, Nada há de oculto que não venha a revelar-se. O contributo do estudo material para a desconstrução do códice 99 do Fundo da Manizola, in: A. Claro, T. Ferreira, T. Reis Miranda, M. Nunes (Eds.), *Orthogr. Arith. Siencias* - Três Tratados Do P.e António Pessoa (c. 1648 S.J.), 1st ed., Lisboa, Scribe, 2023, pp. 19–44.
[16] B. Reissland, J. Hofenk de Graaff, Condition rating for paper objects with iron–gall ink, Netherlands Inst. Cult. Herit. (2001) 1–4.
[17] M. Nunes, J.Costa Vieira, A.P. Costa, M.E. Cabral, B.J.C. Vieira, J.C. Waerenorgh, H.I.S. Nogueira, S.G. Mitchell, A. Claro, T. Ferreira, From ink to mockup: a chemical and physical investigation of historical gall ink formulations and their degradative effect on paper support, Chempluschem 91 (2026), doi:10.1002/cplu.202500369.
[18] V. Karpenko, J.A. Norris, Vitriol in the history of chemistry, Chem. List. 96 (2002) 997–1005.
[19] C. Remazeilles, V. Rouchon-Quillet, J. Bernard, T. Calligaro, J.C. Dran, L. Pichon, J. Salomon, M. Eveno, Influence of gum arabic on iron-gall ink corrosion part II: observation and elemental analysis of originals, Restaurator 26 (2005) 118–133.
[20] H. Hapidin, H. Abdullah, I.Nirwana Soelaiman, The potential role of *Quercus Infectoria* gall extract on osteoblast function and bone metabolism, Open J. Endocr. Metab. Dis. 02 (2012) 82–88, doi:10.4236/ojemd.2012.24013.
[21] H. De La Codre, M. Radepont, J.-P. Échard, O. Belhadj, S. Vaiedelich, V. Rouchon, J.-P. Echard, The use of XRF imaging for the chemical discrimination of iron-gall ink inscriptions: a case study in Stradivari's workshop, X-Ray Spectrom 50 (2021) 244–252 1–0, doi:10.1002/xrs.3160.

[22] O. Hahn, B. Kanngießer, W. Malzer, O. Hahn, B. Kanngie, J. Wolfgang, X-ray fluorescence analysis of iron gall inks, pencils and coloured crayons, Stud. Conserv. 50 (2005) 23–32, doi:10.1179/sic.2005.50.1.23.
[23] T.P. Silva, J.X. Matos, D. de Oliveira, I. Morais, P. Gonçalves, L. Albardeiro, F. Carvalho, U.D. Menda, J.P. Veiga, Orange pickeringite from the algares 30-level adit, Aljustrel mine, Iberian pyrite belt, Portugal, Minerals 11 (2021) 1115, doi:10.3390/min11101115.
[24] F. Frau, The formation-dissolution-precipitation cycle of melanterite at the abandoned pyrite mine of Genna Luas in Sardinia, Italy: environmental implications, Mineral. Mag. 64 (2000) 995–1006, doi:10.1180/002646100550001.
[25] O. Hahn, W. Malzer, B. Kanngiesser, B. Beckhoff, Characterization of iron-gall inks in historical manuscripts and music compositions using X-ray fluorescence spectrometry, X-Ray Spectrom 33 (2004) 234–239, doi:10.1002/xrs.677.
[26] W. Malzer, O. Hahn, B. Kanngiesser, A fingerprint model for inhomogeneous ink-paper layer systems measured with micro-X-ray fluorescence analysis, X-Ray Spectrom 33 (2004) 229–233, doi:10.1002/xrs.676.
[27] I. Arcon, J. Kolar, A. Kodre, D. Hanzel, M. Strilc, XANES analysis of Fe valence in iron gall inks, X-Ray Spectrom 36 (2007) 199–205, doi:10.1002/xrs.962.
[28] M. Karamać, Chelation of Cu(II), Zn(II), and Fe(II) by tannin constituents of selected edible nuts, Int. J. Mol. Sci. 10 (2009) 5485–5497, doi:10.3390/ijms10125485.
[29] M. Manso, A.M. Cardeira, M. Silva, A. Le Gac, S. Pessanha, M. Guerra, A.T. Caldeira, A. Candeias, M.L. Carvalho, The mysterious halos in iron gall ink manuscripts: an analytical explanation, Appl. Phys. A Mater. Sci. Process. 118 (2015) 1107–1111, doi:10.1007/s00339-014-8924-z.
[30] T. Čechák, T. Trojek, L. Musílek, H. Paulusová, Application of X-ray fluorescence in investigations of Bohemian historical manuscripts, Appl. Radiat. Isot. 68 (2010) 875–878, doi:10.1016/j.apradiso.2009.10.039.
[31] G. María, C. Zamorano, Evolución de la composición de las tintas ferrogálicas a trvés de las fuentes documentales de lis siglos XIII al XIX, Estud. Hist. y Patrim. La Edad Media. XIII (2022) 34–67.
[32] C. Vuillard, M. Radepont, F. Téreygeol, C. Remazeilles, V. Rouchon, From experimental archaeology to laboratory: mineralogical nature and elemental composition of medieval manufactured vitriols, J. Archaeol. Sci. Reports. 55 (2024) 104460, doi:10.1016/j.jasrep.2024.104460.
[33] A. Lerf, F.E. Wagner, M. Dreher, T. Espejo, J.L. Pérez-Rodríguez, Mössbauer study of iron gall inks on historical documents, Herit. Sci. 9 (2021) 1–14, doi:10.1186/s40494-021-00522-3.
[34] F.E. Wagner, A. Lerf, Mössbauer spectroscopic investigation of FeII and FeIII 3,4,5-trihydroxybenzoates (gallates) - proposed model compounds for iron-gall inks, Zeitschrift Fur Anorg. Und Allg. Chemie 641 (2015) 2384–2391, doi:10.1002/zaac.201500532.
[35] A. Ponce, L.B. Brostoff, S.K. Gibbons, P. Zavalij, C. Viragh, J. Hooper, S. Alnemrat, K.J. Gaskell, B. Eichhorn, Elucidation of the Fe(III) gallate structure in historical iron gall ink, Anal. Chem 88 (2016) 5152–5158, doi:10.1021/acs.analchem.6b00088.
[36] A. Lerf, F.E. Wagner, Model compounds of iron gall inks – a Mössbauer study, Hyperfine Interact 237 (2016) 13–18, doi:10.1007/s10751-016-1280-y.
[37] C.H. Wunderlich, R. Weber, G. Bergerhoff, Über Eisengallustinte, ZAAC - J. Inorg. Gen. Chem. 598 (1991) 371–376, doi:10.1002/zaac.19915980134.
[38] S. Caterino, I.M. Caniola, M. Pignitter, A. Zoleo, C. Crestini, S. Sanchez-Cort, K. Sterflinger, F. Cappa, A systematic multianalytical approach in the study of iron – polyphenolic complexes in iron-gall inks: exploring the potentialities of raman and electron paramagnetic resonance, Inorg. Chem. 64 (2025) 4802–4816, doi:10.1021/acs.inorgchem.4c04232.
[39] J. Gust, J. Suwalski, Use of Mössbauer spectroscopy to study reaction products of polyphenols and iron compounds, Corrosion 50 (1994) 355–365, doi:10.5006/1.3294344.
[40] J. Xiao, C. Wang, S. Lyu, H. Liu, C. Jiang, Y. Lei, Enhancement of Fenton degradation by catechol in a wide initial pH range, Sep. Purif. Technol. 169 (2016) 202–209, doi:10.1016/j.seppur.2016.04.031.
[41] H. Kipton, J. Powell, M.C. Taylor, Interactions of iron(II) and iron(III) with gallic acid and its homologues: a potentiometric and spectrophotometric study, Aust. J. Chem. 35 (1982) 739–756, doi:10.1071/CH9820739.
[42] N.R. Perron, J.L. Brumaghim, A review of the antioxidant mechanisms of polyphenol compounds related to iron binding, Cell Biochem. Biophys. 53 (2009) 75–100, doi:10.1007/s12013-009-9043-x.
[43] R.C. Hider, Z.D. Liu, H.H. Khodr, Metal chelation of polyphenols, Methods Enzymol 335 (2001) 190–203, doi:10.1016/S0076-6879(01)35243-6.
[44] R. Hider, A. Mohd-Nor, J. Silver, Model compounds for microbial iron-transport compounds. Part I. Solution chemistry and Mössbauer study of iron(II) and iron(III) complexes from phenolic and catecholic systems, J. Chem. Soc. Dalt. Trans. (1981) 609–622, doi:10.1039/DT9810000609.
[45] F. Pinzari, B. Gutarowska, Extreme colonizers and rapid profiteers: the challenging world of microorganisms that attack paper and parchment, 2021. https://doi.org/10.1007/978-3-030-69411-1_4.
[46] M.V. Dutton, C.S. Evans, Oxalate production by fungi: its role in pathogenicity and ecology in the soil environment, Can. J. Microbiol. 42 (1996) 881–895, doi:10.1139/m96-114.
[47] N. Ferrer, M. Sistach, Analysis of sediments on iron gall inks in manuscripts, Restaurator 34 (2013) 175–193, doi:10.1515/res-2013-0010.
[48] M.C. Biesinger, B.P. Payne, A.P. Grosvenor, L.W.M. Lau, A.R. Gerson, R.S.C. Smart, Resolving surface chemical states in XPS analysis of first row transition metals, oxides and hydroxides: cr, Mn, Fe, Co and Ni, Appl. Surf. Sci. 257 (2011) 2717–2730, doi:10.1016/j.apsusc.2010.10.051.
[49] A.P. Grosvenor, B.A. Kobe, M.C. Biesinger, N.S. McIntyre, Investigation of multiplet splitting of Fe 2p XPS spectra and bonding in iron compounds, Surf. Interface Anal. 36 (2004) 1564–1574, doi:10.1002/sia.1984.
[50] B. Xing, N. Graham, W. Yu, Transformation of siderite to goethite by humic acid in the natural environment, Commun. Chem. 3 (2020) 1–11, doi:10.1038/s42004-020-0284-3.
[51] S. Chenakin, N. Kruse, Applied Surface Science XPS characterization of transition metal oxalates, Appl. Surf. Sci. 515 (2020) 146041, doi:10.1016/j.apsusc.2020.146041.
[52] J. Heuer, J. Stubbins, An XPS characterization of $FeCO_3$ films from CO_2 corrosion, Corros. Sci. 41 (1999) 1231–1243, doi:10.1016/S0010-938X(98)00180-2.
[53] M. Descostes, F. Mercier, N. Thromat, C. Beaucaire, M. Gautier-Soyer, Use of XPS in the determination of chemical environment and oxidation state of iron and sulfur samples: constitution of a data basis in binding energies for Fe and S reference compounds and applications to the evidence of surface species of an oxidized py, Appl. Surf. Sci. 165 (2000) 288–302, doi:10.1016/S0169-4332(00)00443-8.
[54] D. Mauro, C. Biagioni, M. Pasero, Crystal-chemistry of sulfates from apuan alps (Tuscany, Italy). I. Crystal structure and hydrogen bond system of melanterite, $Fe(H_2O)_6(SO_4)\cdot H_2O$, Period. Di Mineral 87 (2018) 85–92, doi:10.2451/2018PM759.
[55] G.C. Allen, K.R. Hallam, Characterisation of the spinels $M_xCO_{1-x}Fe_2O_4$ (M=Mn, Fe or Ni) using X-ray photoeletron spectroscopy, Appl. Surf. Sci. 4332 (1996) 25–30.
[56] A. Atrei, B. Lesiak-Orlowska, J. Tóth, Magnetite nanoparticles functionalized with citrate: a surface science study by XPS and ToF-SIMS, Appl. Surf. Sci. 602 (2022), doi:10.1016/j.apsusc.2022.154366.
[57] The University of Chicago Library, Iron Gall ink, Art Sci. B. Conserv. (2019) 1–2.
[58] V. Corregidor, R. Viegas, L.M. Ferreira, L.C. Alves, Study of iron gall inks, ingredients and paper composition using non-destructive techniques, Heritage 2 (2019) 2691–2703, doi:10.3390/heritage2040166.